# Finite element model creation and stability considerations of complex biological articulation: the human wrist joint.

**Magnús K. Gíslason[1], Benedict Stansfield[2], David H. Nash[1]**

1. University of Strathclyde, Department of Mechanical Engineering
2. Glasgow Caledonian University, School of Health and Social Care

*Corresponding author. Department of Mechanical Engineering, James Weir Building, University of Strathclyde, 75 Montrose Street, Glasgow, G1 1XJ, UK.

Tel.: +44 (0) 141 548 2313; fax: +44 (0) 141 552 5105

*E-mail address*: magnus.gislason@strath.ac.uk

**Abstract**

The finite element method has been used with considerable success to simulate the behaviour of various joints such as the hip, knee and shoulder. It has had less impact on more complicated joints such as the wrist and the ankle. Previously published finite element studies on these multi bone joints have needed to introduce un-physiological boundary conditions in order to establish numerical convergence of the model simulation. That is necessary since the stabilising soft tissue mechanism of these joints is usually too elaborate in order to be fully included both anatomically and with regards to material properties. This paper looks at the methodology of creating a finite element model of such a joint focussing on the wrist and the effects additional constraining has on the solution of the model. The study shows that by investigating the effects each of the constraints, a better understanding on the nature of the stabilizing mechanisms of these joints can be achieved.

## 1. INTRODUCTION

The finite element method has been employed with considerable success to explore load distribution and deformation patterns at a variety of locations in the human body. The application of the method has been particularly successful in joints with relatively simple geometry and well defined loading conditions, such as the hip[1,2]. The development of an understanding of the aetiology of pathology and the ability to predict the consequences of surgical intervention have been possible using these methods. Other joints that have also been analysed extensively using computational methods include the knee, spine and shoulder. The finite element method has had less impact on knowledge of the mechanics of multi-bone joints such as the wrist and ankle. Both these joints consist of a high number of bones which interact in a unique manner in order to produce overall movement. Within the wrist and ankle there are several challenges for the modelling community including the large number of articulations, complex geometry, non linear properties of supporting soft tissue structures and the inter-relationship between all of these components. It is not surprising therefore that there is considerably less literature concerning wrist and ankle joint finite element modelling than there is for the less complex joints. Additional contributing factor to this lack of literature are that hardware computational speed has only recently developed to the point where full, geometrically accurate, models are feasible except on very high specification machines and that medical imaging methods have only recently become available to readily provide images suitable for creating accurate models.

The current study will concentrate on the development of finite element modelling methods in the wrist joint. The wrist joint is one of the most complex composite articulations in the body. It comprises of 8 carpal bones and their articulations to the two forearm bones and the 5 metacarpals. The carpal bones are, according to classical anatomy, aligned in two rows, the proximal row and the distal row. In the proximal row there are four bones: scaphoid, lunate, triquetrum and pisiform and in the distal row the bones are: trapezium, trapezoid, capitate and hamate (figure 1).

Only a small number of studies have presented analysis of the load transfer through the wrist. For example Nedoma[3] and Schuind[4] present studies using simplified representations of the joint structures. The finite element method has been applied, but again due to the complexity of the articulations, geometrical simplification of the joint and its structures has been used. In 1995, Anderson et al[5] created a plane strain model of the radiocarpal joint which consisted of the radius, scaphoid and the lunate. This was one of the first attempts to address the loading on the radiocarpal joint using finite element methods. Two-dimensional modelling was used throughout. The output from 2D models offers some insight into load transfer, but must be treated with caution. In 2005[6] further enhancements were made to the model, making it three-dimensional with improved contact modelling, however only a sub-section of the wrist was studied.

In 1999 Ulrich et al[7] attempted to prepare an accurate and highly detailed description of the bone geometry by converting CT voxels directly to brick elements within their model. They captured the distal part of the radius, the scaphoid and the lunate with a voxel size of 165 μm in all three dimensions. A model with 1.7 million elements was created. Whilst this approach generated an accurate geometrical representation, there still remained issues associated with the need to smooth the bone surface and the huge number of elements would have made

extension to the whole joint difficult. The publication by Ulrich et al highlights another difficulty in modelling of complex joints; that of defining the loading applied at the boundaries of the model. It appeared that a combined loading of 1000N was applied in an ad-hoc manner onto the scapho-capitate and luno-capitate articulations. Justification for boundary condition loading is sometimes entirely absent or based on estimates from the literature, e.g. forces calculated using biomechanical models as exemplified in Chadwick et al for maximal griping[8]. Ulrich et al provide little detail of the contact modelling approach employed.

The wrist and ankle are similar in overall structural complexity. Methods applied in the development of finite element models should be transferable between the two joints. In 2001 and 2003 Chen et al[9,10] presented a finite element model of the ankle. Their model fused together blocks of bones, merging them together with surrounding soft tissue for stability. In 2004 Cheung et al[11] created a more refined model of the ankle, allowing articular contact between 28 bony segments, where stability was achieved through truss elements representing ligaments and the fascia. Few studies have attempted to model the whole wrist structure and simulate physiological loading in the same way as Cheung did for the foot.

In 2003 Carrigan et al[12] created a three-dimensional model of all the carpal bones and the radius and ulna but excluded the metacarpals. All major ligaments were modelled with spring elements. Non-physiological loading was applied of 15 N compressive force acting on the distal surface of the capitate. In 2009 a similar model was presented by Guo et al[13], with a full model of the wrist, including the metacarpal bones and the transverse carpal ligament.

Establishing physiological boundary conditions is a particular challenge especially for partial models of the wrist were internal loads are poorly documented. Another issue is the application of un-physiological constraints in order to achieve convergence. The wrist bone structure is highly unstable without constraints which are provided from surrounding soft tissues such as ligaments, tendons and muscles. These tend to be ignored in many studies. In some cases further constraints are needed to achieve convergence pointing to the fact that other mechanisms play a significant role in the stabilization of such a multi-bone analysis. Guo et al[13] solved the dorsal/palmar and radial/ulnar instability in the wrist by applying boundary conditions on all the carpal bones apart from the scaphoid, constraining their motion to only allow proximal/distal displacement of the bones. Carrigan et al[12] approached the stability problem by drastically increasing the ligament stiffness after exceeding a given strain value as well as placing boundary conditions on the scaphoid.

Previous attempts at wrist modelling have not overcome the problems associated with the inherent instability of the bones. Finite element analysis of the complex structures at the wrist joint has not been previously performed using physiologically reasonable loading where a particular function of the hand was under observation.

In this study a finite element model of the wrist is developed which addresses the issues of bone geometry and interaction, constraints and contact modelling, mesh refinement and convergence and in addition physiologically reasonable loading is applied at the boundaries. The details presented provide a guide for developers of finite element applications in complex joints of the human body and demonstrate how additional constraints affect the model solution.

## 2. METHODS

**2.1 Defining the geometry**

The geometrical representation of the model was obtained by MRI scans. The scans were taken of the wrist, ranging from the distal end of the two forearm bones, radius and ulna, to the proximal third of the metacarpals. The total length of the scans was 63.9 mm. The resolution of the scans was 234 µm in plane and the slice thickness was 750 µm. The scans were imported into Mimics (Materialise, Belgium) where the edge detection was carried out for each of the 14 bones using the 'masking technique', which involved masking out each pixel belonging to each bone within a given slice (Figure 2). The contours of each slice were then reconstructed into a 3-dimensional object. The geometrical creation was an integral part of the finite element modelling, particularly with reference to the numerous articulating joints in the wrist. After the geometrical objects had been created, the geometrical interaction between each set of bones was investigated. Where bone articulations were not morphologically accurate, the masks of the corresponding bones were recalculated based on the interacting three-dimensional objects and further enhancement carried out on the masks to create an improved fit between the contact surfaces. The object was then meshed using a semi-automatic mesher incorporated in Mimics. The surfaces were meshed using triangular surface elements. Various normalized indicators were used to verify the mesh such as the ratio between the inscribed and ascribed circle and the skewness defined as the ratio between the triangle and an equilateral triangle with the same ascribed circle and the equi-angle skewness which was defined as

$$\min\left(\frac{\alpha}{60};\frac{180-\beta}{180-60}\right) \qquad (1)$$

where $\alpha$ was the smallest angle of the triangle and $\beta$ was the largest angle of the triangle[14]. Ideally the ratios would be unity, but the lowest value was set at 0.4. This was carried out according to recommendations[15] that the minimum equi-angle skewness value is proposed to lie between 0.4 and 0.5 in order to create a high quality surface mesh. Automatic smoothing steps were carried out on the bone geometry by re-arranging the position of each node point relative to its nearest neighbours in order to remove any local sharp edges. The volume changes within the bones were compensated for in Mimics by repositioning of the node points.

The surface mesh was imported into Abaqus (Simulia, version 6.7) where volume elements were created by filling the void of each of the bones using a subroutine in Abaqus which converted the surface triangular elements into tetrahedral elements, C3D4. Further checks, such as verification of the elements' aspect ratio and shape factor were carried out on the volumetric elements in order to further address the element quality. The mesh was exported back into Mimics where the elements were assigned material properties with the visual aid of the MRI scans. The MRI scans were not of sufficient resolution to allow precise property assignment based on grey scale values, but were used to check that estimates used were suitable for the specific geometry under study. The cortical shell is relatively uniform in the carpal bones and forearm bones with an average thickness of 2.6mm in the radius[16].The shell thickness was simulated using Mimics, by performing an erosion of the current mask by 10 pixels where each pixel was 0.23mm in size and subtracting the new mask from the original mask, the remainder was a shell like structure representing the cortical bone. The pixels belonging to each of the two different stiffness regions of the hard cortical shell and the soft cancellous bone were well defined on the MRI scans and were projected onto the volumetric mesh and the material properties were calculated based on the majority of voxels belonging to each mask. This proved to be a very time efficient method of defining the stiffness regions and incorporating the material properties onto the volumetric mesh. After the assignment of the material properties, the meshes were exported and re-imported into Abaqus.

Deleted: based on

Attempts were made to model the cartilage distribution by identifying elements of the model that were within the cartilage zone on the MRI scans. However, this was not successful as the edge of the area defined using this method followed element boundaries and was therefore not smooth, leading to unanatomical protrusions of cartilage into bone and visa a verse. The cartilage was created by manually identifying the articulating surfaces on the bones and extruding the elements and forming wedge elements of cartilage (C3D6). This resulted in a good geometrical representation and material distribution of the cartilage. Figure 3 illustrates the complete model.

### 2.2 Meshing the bone: Orphan meshes vs. geometric entities

It was decided to mesh the bones within Mimics and export from there instead of building a geometric object from the outlines of each bone. By meshing within Mimics it was possible to easily control the density of the surface mesh. At contact areas the mesh density could be increased and where low stress concentrations were expected the density could be decreased. Manual creation of surface elements and node points was also used when considered necessary. The balance between high mesh density at contact points and lower density in other areas was essential to keep the number of elements to manageable levels. The finite element model was built up by converting the surface meshes into tetrahedral elements. Due to this direct relationship between surface and volume mesh, care needed to be taken when the surface mesh was tightened at the articulating surfaces, as too fine a surface mesh would result in an excessively high number of tetrahedral elements. Another aspect of importing orphan meshes into Abaqus rather than creating geometry directly was the fact that once the structure had been imported, little could be done to change parameters within the structure. This made the process of creating a well balanced surface mesh even more important. Creating the mesh outside Abaqus made the process more time efficient without compromising the geometrical integrity.

### 2.3 Contact modelling

A surface-to-surface contact was established between the articulating surfaces using the 'hard contact' algorithm based on[17]:

$$p = 0, \; for \; h < 0$$
$$h = 0, \; for \; p > 0$$

where $p$ was the contact pressure and $h$ was the overclosure between the surfaces. The contact modelling was implemented in Abaqus code and the kinematic contact algorithm used. This was preferred to the penalty contact since it would introduce additional stiffness to the system. Frictionless contact properties were also implemented on the articulating surfaces. By using frictionless contact, it was ensured that no shear stresses occured at the articulations.

It has been reported in the literature[18,19] that there is little or no movement between certain articulations, such as the articulations between the bones in the distal row of the wrist. Table 1 shows the specific articulations which were assumed to have little motion between them. The node points in those articulations were tied together, not allowing any motion between the bones.

| Articulations | Type of contact |
|---|---|
| Radius-ulna | Contact |
| Radius-scaphoid | Contact |
| Radius-lunate | Contact |
| Scaphoid-capitate | Tie |
| Scaphoid-trapezium | Contact |
| Scaphoid-trapezoid | Contact |
| Lunate-capitate | Tie |
| Lunate-triquetrum | Contact |
| Triquetrum-hamate | Contact |
| Hamate-capitate | Contact |
| Capitate-trapezoid | Tied |
| Trapezoid-trapezium | Tied |
| Distal row - metacarpals | Tied |

**Table 1**: Types of contact between listed articulations

### 2.4 Tissue properties modelling

#### *2.4.1 Bone and cartilage*

The cortical and cancellous bones were modelled using linear, isotropic material properties with Young's modulus of 18 GPa and 100 MPa respectively[20, 21]. The range of values in the literature for the Young's modulus of bone is great. Nearly all finite element studies carried out on joint mechanics have modelled bone as a linear isotropic material. The Poisson's ratio values used were 0.2 for cortical bone and 0.25 for cancellous bone. The cartilage was modelled using hyper-elastic material properties as has been proposed by Brown et al[22], which are suited to large deformation cartilage behaviour modelling since linear elastic material is only intended to accurately predict behaviour to around 5% elastic strain. The hyperelastic model used was a two parameter Mooney-Rivlin type, with coefficients obtained from Li et al[23] who proposed the parameters making up the curve should be $C_{10}$=4.1 MPa and $C_{01}$=0.41 MPa. The stress strain curve for the cartilage obtained through this modelling is similar to the findings presented by Finlay and Repo[24] testing knee articular cartilage and Leanne and Aspden[25] testing bovine articular cartilage.

Deleted: .

Deleted: [22]

Deleted: .

#### *2.4.2 Ligament*

The ligaments were modelled with non-linear spring elements (CONN3D2) where the position of the insertion points was estimated from previously published anatomical studies [24] and the Interactive Hand multimedia CD (Primal Pictures) [25]. Distributed origins and insertions of the ligaments were simulated by applying multiple springs in parallel. The material properties were estimated from previously published papers[26-28]. Reported ultimate load and strain were used to recreate tensile characteristic curves of the ligaments using Matlab (Mathworks).

The non linear curves of the ligaments were generated using the following criteria: With zero or negative force there was no strain. The non-linear toe region was estimated at 15% of the maximum strain $\varepsilon_{ref}$. Finally a linear curve from the 15% maximum strain to maximum strain with the same slope at the boundary between the linear and nonlinear regions was created based on the formula derived from Logan and Nowak[28]

$$F = \begin{cases} \dfrac{\alpha x^2}{2\varepsilon_{ref}}, & 0 \le x \le \varepsilon_{ref} \\ ax + b, & x \ge \varepsilon_{ref} \end{cases}$$

where $F$ was the ligament force, $x$ the strain and α, $a$ and $b$ constants.

### 2.5 Specification of loading conditions

The loading on the finite element model was acquired through a biomechanical study. The gripping strength of the subject was measured using five 6 degrees of freedom force transducers (Nano 25-E and Nano 17, ATI Industrial Automation Inc, USA). Simultaneous collection of motion/position data using an 8 camera motion capture system (Vicon, Oxford Metrics Ltd) allowed the determination of kinetic and the kinematic data. The measured external forces were converted into joint contact forces on the metacarpals using an inverse dynamic biomechanical model as described by Fowler and Nicol[29, 30]. The contact forces were applied as compression in the direction of each metacarpal bone. Loading was applied to the distal ends of all the metacarpals through a predefined subset of nodes in order to minimize the effects of point loading on the solution.

Thus a set of loading conditions with a physiological justification were used representing the task of griping. The loading was applied in a smooth step over the whole simulation time. The smooth step defined an amplitude, '$a$', between two data point ($t_i$,$A_i$) and ($t_{i+1}$, $A_{i+1}$), using the formula[17]

$$a = A_i + (A_{i+1} - A_i)\xi^3(10 - 15\xi + 6\xi^2), \qquad t_i \le t \le t_{i+1}$$

where

$$\xi = \frac{t - t_i}{t_{i+1} - t_i}$$

As a result of the interpolation function, the first and second derivatives were 0 at both $t_i$ and $t_{i+1}$. This controlled the rate of load application and minimized the risk of any dynamic effects which might have compromised the assumption of a quasi-static behaviour.

### 2.6 Model constraints

The proximal ends of the radius and ulna were fully constrained and not allowed to translate or rotate. Additionally further constraints were applied to the model to add stability and aid convergence.

The initial constraints on the model were the following:

- Metacarpal movement was constraint by placing rigid connectors between them.
- The carpo-metacarpal joint was tied.
- Infinitely stiff radio-collateral ligaments on the radial aspect were specified.
- The proximal insertion points of the five tendons modelled were fixed.
- The scaphocapitate and capitolunate joints were tied.

It was assumed that during the static gripping task modelled that there would be no relative movement between the metacarpals and the distal row of the carpal bones due to the stout ligaments connecting the metacarpals to each other and to the distal row. The geometrical shape of the carpometacarpal joint also plays a part in joint stability. This applies in particular to the 2nd and 3rd metacarpal, whereas the 4th and 5th are more mobile[31].

The origins of the tendons on the radius were outside the volume modelled. The tendons' proximal ends were constrained in association with the radius. The insertion points of the other tendons were obtained from Horii[32].

The constraining effect of the radiocollateral ligament was necessary to act against the contact forces from the first metacarpal, which tended to push the carpus ulnarly resulting in excessive translation of the scaphoid and lunate which was not thought to represent physiological behaviour.

The scaphocapitate and the capitolunate articulations are highly unstable joints, stabilised primarily by the radiocapitate ligament and other soft tissue mechanism[33]. It was initially assumed that these joints were tied together in order to aid convergence.

**2.7 Finite element solver**

The model was solved using Abaqus Explicit. The explicit algorithm made the contact modelling extremely robust. The solution for timestep $t+\Delta t$ was based on the status of the model at the previous time step, $t$. In contrast for the implicit code the solution is based on the same time step. It has been demonstrated that non-linearities can cause divergence using the implicit code[34]. The time step in the explicit analysis was determined from the characteristic element length and material properties. The time step was given by[17]

$$\Delta t \leq \frac{2}{\omega_{max}}$$

where $\omega_{max}$ was the maximal eigenvalue in the system. In Abaqus the inequality was evaluated using the following expression

$$\Delta t = \min\left(\frac{L_e}{c_d}\right)$$

Where $L_e$ was the characteristic element dimension and $c_d$ was the dilatational wave speed of the material, defined as

$$c_d = \sqrt{\frac{\bar{\lambda} + 2\bar{\mu}}{\rho}}$$

where $\bar{\lambda}$ and $\bar{\mu}$ were known as the Lamé constants, defined as

$$\bar{\lambda} = \frac{Ev}{(1+v)(1-2v)}$$

$$\bar{\mu} = \frac{E}{2(1+v)}$$

where $E$ was the Young's modulus and $v$ was the Poisson's ratio. The minimum time steps in the analysis were of the magnitude of $10^{-8}$ s/increment. The quasi-static modelling required

that the kinetic energy did not exceed 5% of the strain energy in order to exclude any dynamic behaviour[34]

## 3. RESULTS

### 3.1 Model quality indicators

The total number of elements for the whole structure was 430,306, with an element density of 10.0 elements/mm$^3$. The analysis was carried out using the Abaqus Explicit code on a 4 node high performance computer (HPC) cluster with dual processors (2.0 GHz) running with 32Gb memory. An average CPU time for solving each simulation was 242 hours. The analysis was run over a simulation time period of 0.01s.

The ratio between inscribed and ascribed circle for 67.9% (std=3.8%) of elements was greater than 0.95 (where unity represents an equilateral triangle) and 96.6% (std=2.1%) greater than 0.85, confirming the high quality of the surface elements.

A comparison was made between the kinetic and strain energy to verify that limited inertial effects were present. The model converged with kinetic energy which was 3.9% of the total strain energy at the end of the load step. Thus the assumption of a quasi static behaviour was justified. The energy graph can be seen in Figure 4. In addition to comparing the internal energy to the kinetic energy to validate the quasi static behaviour of the model, the input forces against the output forces were calculated and compared. A maximum of 2% error between the output forces and the input forces was obtained indicating a good level of solution convergence

Deleted: less than 5%

.

### 3.2 Model boundary loading

The load calculated using the biomechanical model was used to derive a loading at the boundaries. Within the biomechanical model it was assumed that there were no rotational loading at the joint contacts, only compressive and shear loadings on the bones. The joint forces were calculated at the level of the MCP joint. The compressive forces were applied as loading conditions on the finite element model with resultant force of 647.5 N in magnitude, distributed over the 5 digits, applied on the metacarpals. The thumb and the index finger carried the largest loads (Table 2). This loading condition simulates half of the maximum gripping force generated by the subject. Other load cases can be found in Gislason et al 2009[35] where comparison was made between the load transfer in various subjects and in various positions of the wrist.

| | Thumb | Index | Long | Ring | Little |
|---|---|---|---|---|---|
| Loading [N] | 255.6 | 120.3 | 106.4 | 88.0 | 77.3 |

Table 2: Relative loading on the metacarpal bones

### 3.3 Bone stress

Stress plots were created of the wrist bones and the load transfer characteristics observed. A stress plot of the wrist assembly can be seen in Figure 5. From the stress plots it could be seen that the highest stresses occurred at the thin cortical shell and were, on average, an order of magnitude higher than the stresses in the softer cancellous bone. On average the stresses in the cortical bone in the radius were 18.6 MPa, whereas the stresses in the cancellous bone for the radius were 1.1 MPa.

Deleted: figure
Deleted: 4

The stress distribution through the cancellous bone showed that the load was transmitted in a similar manner as predicted from Hertzian contact theory. This can be seen in Figure 6, where it can also be seen how the stress concentration from the radiocollateral ligaments was transmitted into the cancellous elements.

Deleted: figure
Deleted: 5

### 3.4 Effects of constraints

Conversion of the model was achieved without implementing any of the constraints mentioned above. It was noticed however that with the loss of the radial stabilizers, the displacements of the scaphoid and the lunate became large in palmar and ulnar directions. The loss of the metacarpal ligamentous constraints had minimal effect under the imposed loading conditions. With no constraints other than the tendon fixation points and carpo-metacarpal surface constraints, comparison was made between the location of the centre of pressure at the radiocapal joint with time with and without the loading on the first metacarpal. The progression of the centres of pressure with time can be seen in Figure 7. The centre of pressure travelled ulnarly for both the radioscaphoid and radiolunate articulations under the influence of the loading from the first metacarpal. When the loading was removed from the first metacarpal, the displacement of the centre of pressure became almost entirely palmarly directed.

Deleted: figure
Deleted: 6

### 3.5 Effects of contact modelling method

The model converged after the capito-scaphoid, capito-lunate and capito-trapezoid surface tie constraints were converted into surface to surface contacts. Removing the constraints on the scapho-capitate articulation caused extension and palmar translation of the ulnar side of the carpus. Similar results were obtained when constraints were additionally removed from the capito-lunate articulation. The modelling of the unconstrained capitolunate and scaphocapitate articulations caused the whole carpus to radially deviate compared to the constrained model. Secondary effects of the constraining of the capitolunate and the scaphocapitate articulations were that the scaphoid showed larger displacements of the nodepoints than the unconstrained model, both in ulnar direction and palmar direction. A similar result was found for the lunate, but in the unconstrained model the translation in the palmar direction was higher than for the constrained model, opposite to the scaphoid. In general the scaphoid and lunate showed higher displacements for the constrained model.

### 3.6 Validation

Preliminary validation was carried out in a study run parallel to the modelling at the Bioengineering Unit at the University of Strathclyde. Strain gauges were placed on the scaphoid, lunate, radius and the ulna on cadaveric specimens and the load transfer ratio estimated through these bones using similar loading conditions as described above. The results from the numerical model were in agreement with the cadaveric study, identifying the radius as the significant load bearer in the wrist. Further work is needed to generate sufficient evidence to validate the finite element model.

Deleted: ¶

## 4. DISCUSSION

The work reported here is the first robust attempt at such a detailed three-dimensional finite element model of the wrist with physiologically representative loading conditions. The development of the methods to achieve a successful outcome of the modelling provides useful guidance for others attempting to develop similar models.

Deleted:

Initially attempts were made to carry out the modelling using the implicit solution algorithm. Those attempts were unsuccessful. The limitations of using the implicit method were most clearly seen in high residual forces at the boundaries of the contact surfaces causing the solution to diverge. Attempts were made to incorporate damping between the bones which would be released gradually as the load step progressed and be fully released when 100% of the loading was applied. The load step progressed well at the beginning, but cutbacks started to be seen once the effects of the damping decreased. The cutbacks increased and the solution never reached the end of the load step and represented a classical behaviour of the proper contact not being established between the bones. It was therefore necessary to use the explicit solution algorithm. The time step of the explicit simulation, 0.01s, was determined by balancing the maximum time needed for quasi static energy criteria to be met and the overall physical time needed to solve the model. The CPU time needed was 240 hours, divided on 4 parallel nodes resulted in the model being solved in just over 3 days. By increasing the overall step time, the simulation time would increase accordingly. Increasing the step time to 0.05s showed no significant changes to the model compared to step time of 0.01s.

Initially, various constraints were applied to the wrist such as fixation of the joints, fixed distance between the metacarpals and overly stiff ligaments in order to stabilize the carpus. The influence of these constraints varied on the overall solution. The absence of the fixators between the metacarpals allowed increased movement between the metacarpals, but did not significantly increase the kinetic energy in the model. Should shear forces be introduced (directed dorsally and ulnarly) on the metacarpals, the existence of the metacarpal constraints would have played a much more significant role in stabilizing the structure in order to achieve convergence and prevent excessive translation of the bones[35]. Releasing these constraints gave a better stress distribution over the metacarpals, where local stress hotspots (which died out quickly with distance from the insertion points) were identified with the constraints.

Contact modelling remained frictionless, but a model was simulated, incorporating a friction coefficient of 0.02 which had minimal effect on the overall solution. Previous models incorporated a 'rough' contact model, indicating that once the bones were in contact there was no movement allowed on the contact surface. This kind of modelling yielded high shear stresses on the articulations which were not thought to be representative of physiological behaviour.

Another constraint that was implemented on the model was the high stiffness of the radiocarpal ligament. This constraint was implemented in order to resist the ulnar directed forces coming from the thumb (1st metacarpal) and restraining ulnarly directed movement of the carpal bones. This constraint had a larger impact on the overall solution. When removed, a larger displacement of the scaphoid and the lunate in the ulnar direction was seen. This supports the hypothesis that the soft tissues surrounding the radial side of the wrist play a large role in stabilising the joint, tending to translate the carpal bones ulnarly. This was further displayed when loading was removed from the first metacarpal. The centre of pressure

for the radioscaphoid and radiolunate articulations were translated palmarly under the loading from metacarpals 2-5 opposed to palmar and ulnar translation (seen in Figure 7) when loading was applied to all five metacarpals.

The model presented here constitutes an advancement on those reported in the literature. There are, however, areas where improvement is possible. One physiological loading condition is presented. A wider appreciation of the load bearing requirements would be possible if a variety of loading scenarios were presented. Although an attempt has been made to include all major muscular and ligamentous structures, natural variation in the occurrence and anatomy of these structures should be studied, to establish the effect of such variation on load distribution outcome. Simplification of soft tissue structures has been made with, for example, a finite number of elements representing each ligament's action. A true anatomical representation would include a much larger number of fibres, reducing the concentration of load at the ligament-bone attachment sites.

The effect of simplification of ligament representation was seen at the insertion of the stiff radio-collateral ligaments. Such simplifications led to small areas of unphysiological stress concentration. However, the number of bone elements that carried stresses higher than 50 MPa and were considered outside the physiological range amounted to only 3.5% of the overall element count, indicating that the ligament and surface constraints did not significantly alter the overall stress distribution on the carpal bones.

Although an attempt has been made to include all of the load bearing structures in the model, there is clearly a need to investigate further the restraining role of the ligaments in maintaining the palmar-dorsal alignment of the bones. Resistance to lateral loading was not included within the capabilities of the elements used to model the ligaments.

A key part of the model to ensure integrity of results was the accurate geometrical model of the articulating surfaces. The surfaces on opposing sides of each articulation had to have representative concavity or convexity to eliminate unphysiological stress concentrations developing. The specification of accurate contacting surfaces was critical to the ability of the finite element model to solve as inaccuracies led to element distortion and solution divergence.

## 5. CONCLUSIONS

Physiological loading conditions, based on real measured external loading and position information, were calculated using a biomechanical model of the internal structures of the hand. These physiologically reasonable loads were applied to a geometrically accurate three-dimensional finite element representation of the structures of the wrist to examine the load distribution. Bones, cartilage, ligaments and tendons were all included in the model, thus providing the most accurate estimates of internal loading in the wrist available to date.

The creation of a finite element model of the whole wrist poses many challenges. The work reported here provides guidance for development of modelling methods in terms of definition of anatomical structure, contact modelling and representation of soft tissues. Although it is acknowledged that considerable development remains, it is hoped that the methods described will lead to improved knowledge of internal wrist loading to better inform surgical decision making and a range of other clinical interventions and rehabilitation practices.

## ACKNOWLEDGEMENTS

The authors wish to thank the Furlong Research Charitable Foundation which funded this work.

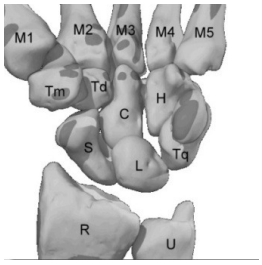


Figure 1a: Bones of the wrist (palmar view)

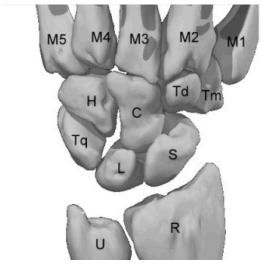


Figure 1b: Bones of the wrist (dorsal view)

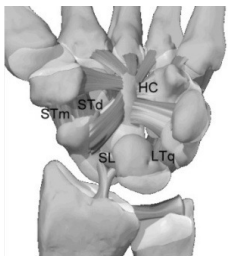


Figure 1c: Deep ligaments of the wrist (palmar view)


Figure 1d: Deep ligaments of the wrist (dorsal view)

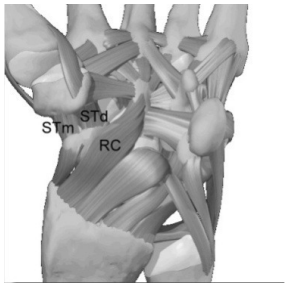


Figure 1e: Superficial ligaments of the wrist (palmar view)

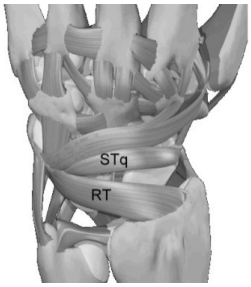


Figure 1f: Superficial ligaments of the wrist (dorsal view)

**Figure 1:** View of the wrist bones and the major ligaments. R=radius, U=ulna, S=scaphoid, L=lunate, Tq=triquetrum, H=hamate, C=capitate, Td=trapezoid, Tm=trapezium, M 1-5=metacarpals 1-5, SL=scapholunate ligament, LTq=lunotriquetral ligament, HC=hamitocapitate ligament, STd=scaphotrapezoid ligament, STm=scaphotrapezium ligament, HTq=hamitotriquetral ligament, RC=radiocapitate ligament, STq=scaphotriquetrum ligament, RT=radiotriquetrum ligament. Images taken

and adapted from Interactive Hand CD (Primal Pictures)[25].

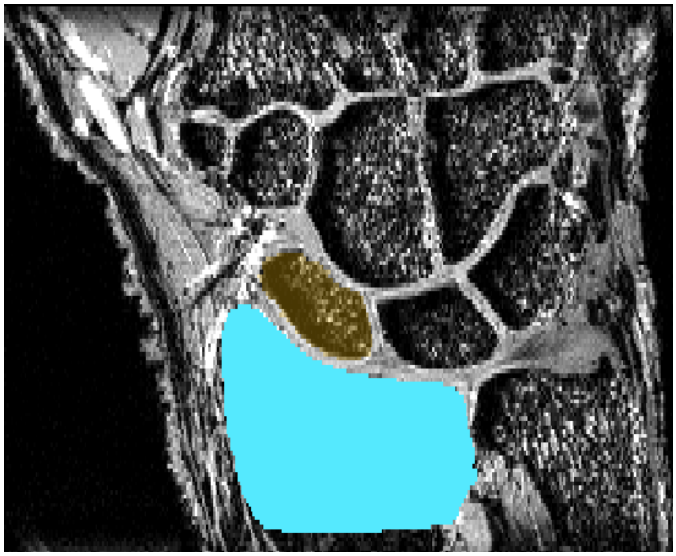

Figure 2: An MRI scan of the wrist with two bones masked.

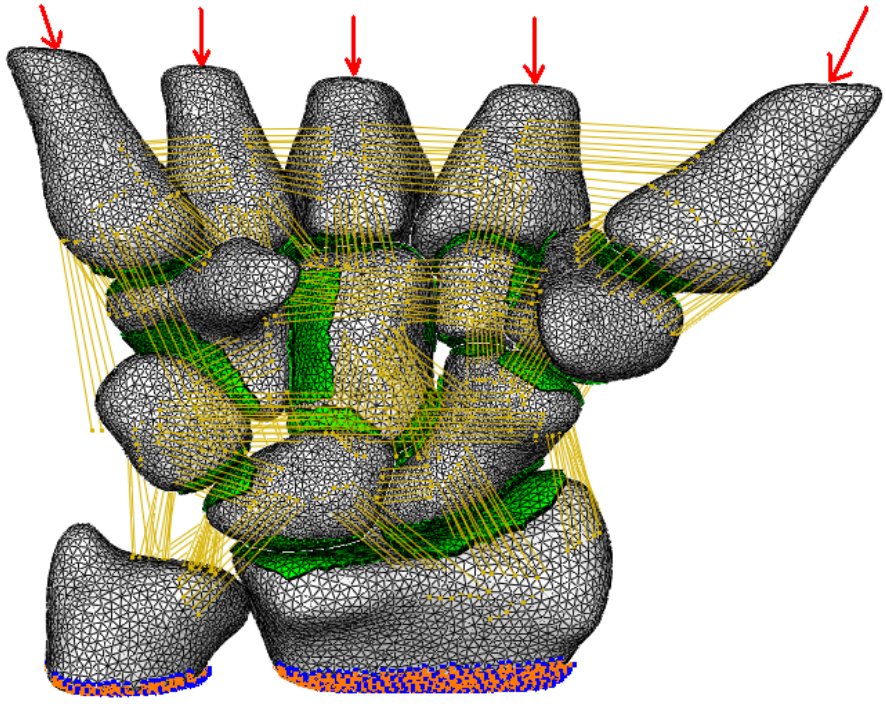

Figure 3: Finite element model assembly. From the figure the proximal fixation and the loading conditions can be seen. The cartilage elements can be seen as the extruded elements at the articulations between the bones. Forces were applied along the metacarpal axis and the proximal ends of the radius and ulna were kept rigid.

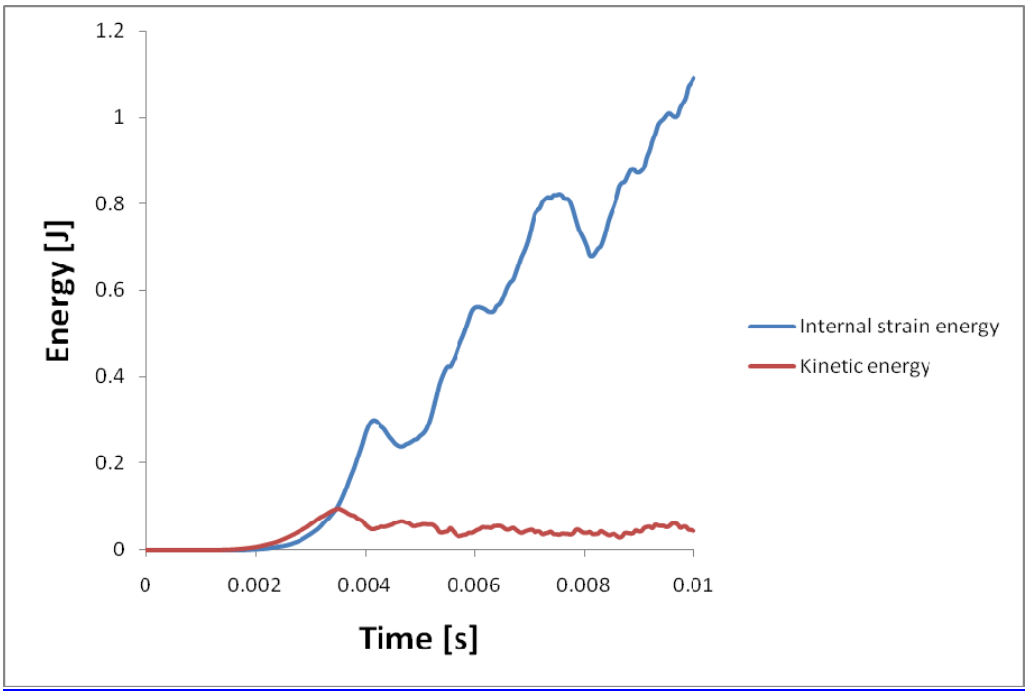


Figure 4: Graph showing total internal strain energy and kinetic energy. It can be seen how the kinetic energy is negligible compared to the internal strain energy, confirming quasi static behaviour.

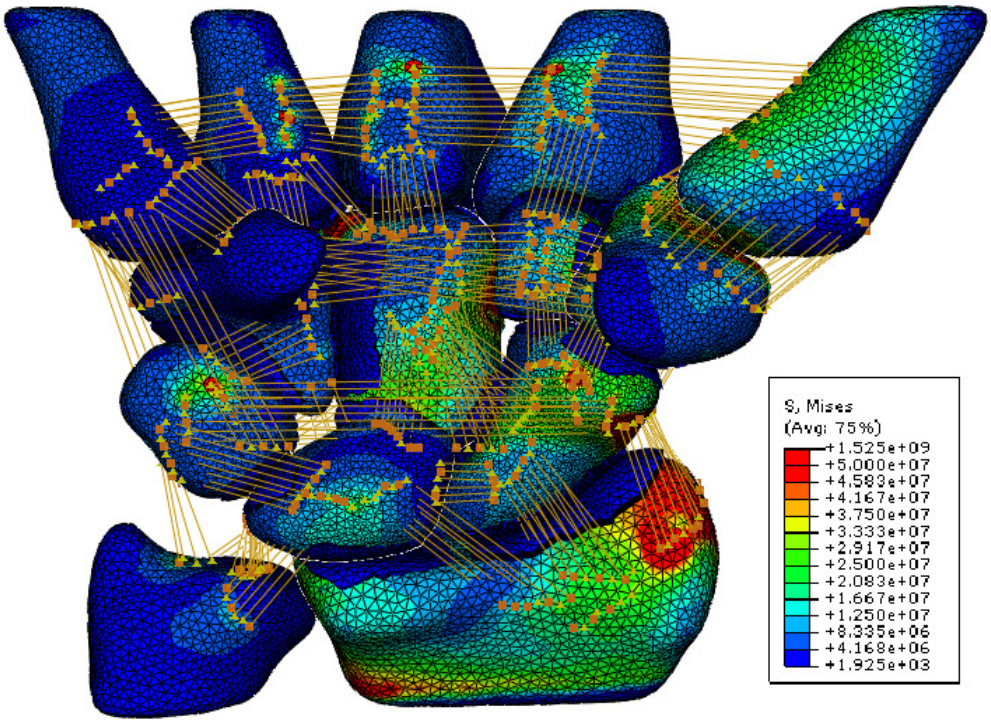


Figure 5: Von Mises stress plots for the whole wrist structure. From the figure it can be seen how the load is primarily transmitted through the radial aspect. Stress concentrations at the ligament-bone connections can be seen, particularly in the constrained radiocollateral ligament. Note the localised nature of these concentrations.

Deleted: 4

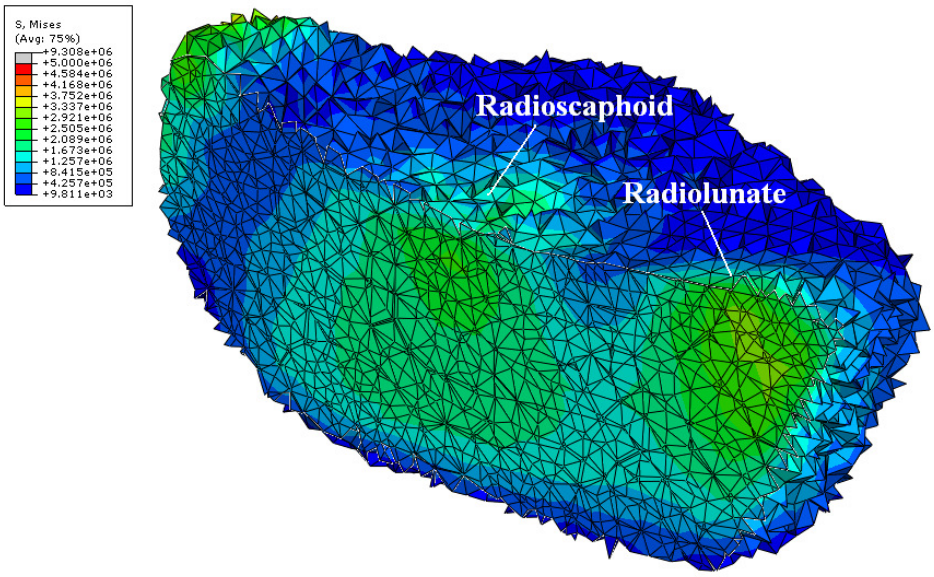


Figure 6: Von Mises stress plots for the internal cancellous bone in the radius showing Hertzian behaviour of the contact modelling

Deleted: 5

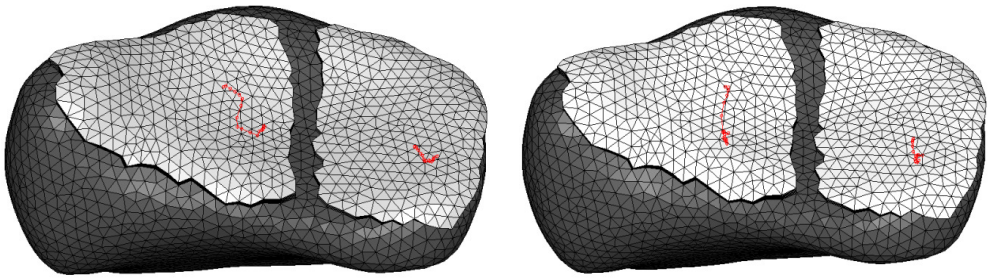

(a) Loading applied on all metacarpals (b) Loading removed from the 1st metacarpal

Figure 7: Progression of the centre of pressure on the radiocarpal joint with time during the explicit solving routine.

Deleted: 6

**REFERENCES**


1. Viceconti, M., Davinelli M., Taddei F. and Cappello A.: Automatic Generation of Accurate Subject Specific Bone Finite Element Models to be Used in Clinical Studies, Journal of Biomechanics, 2004, 37, 1597-1605.

2. Taddei, F., Pancanti A. and Viceconti M.: An Improved Method for the Automatic Mapping of Computed Tomography Numbers onto Finite Element Models, Medical Engineering and Physics, 2004, 26, 61-69.

3. Nedoma J. , Klézl Z., Fousek J., Kestřánek Z., Stehlík J, Numerical Simulation of Some Biomechanical Problems, Mathematics and Computers in Simulation, 2003, 61, 283-295.

4. Schuind, F., Cooney, W.P., Linscheid, R.L., An K.N., and Chao, E.Y.S., Force and Pressure Transmission Through the Normal Wrist: A Theoretical Two-Dimensional Study in the Posteroanterior Plane, Journal of Biomechanics, 1995, 28(5), 587-601.

5. Anderson, D.D. and T.E. Daniel T.E.: A Contact-Coupled Finite Element Analysis of the Radiocarpal Joint, Seminars in Arthroplasty, 1995, 6(1), 30-36.

6. Anderson, D.D., Deshpande, B.R., Daniel, T.E, and Baratz, M.E.: A Three-Dimensional Finite Element Model of the Radiocarpal Joint: Distal Radius Fracture Step-off and Stress Transfer, The Iowa Orthopaedic Journal, 2005, 25, 108-117.

7. Ulrich, D., van Rietbergen, B., Laib, A., and Ruegsegger, P., Load Transfer Analysis of the Distal Radius From In-vivo High Resolution CT-imaging, Journal of Biomechanics, 1999, 32, 821-828.

8. Chadwick, E. and Nicol. A.C.: Elbow and Wrist Joint Contact Forces During Occupational Pick and Place Activities, Journal of Biomechanics, 2000, 33, 591-600.

9. Chen, W.P., Ju, C.W., and Tang, F.T.:. Stress Distribution of the Foot During Mid Stance to Push-off in Barefoot Gait: A 3-D Finite Element Analysis, Clinical Biomechanics, 2001, 16, 614-620.

10. Chen, W.P., Ju, C.W., and Tang, F.T.: Effect of Total Contact Insoles on the Plantar Stress Redistribution: A Finite Element Analysis, Clinical Biomechanics,2003, 18, 17-24.

11. Cheung, J.T.M., Zhang M, Leung A.K. L, and Fan, Y.B.: Three Dimensional Finite Element Analysis of the Foot During Standing: A Material Sensitive Study, Journal of Biomechanics, 2004, 38, 1045-1054.

12. Carrigan, S.D., Whiteside, R.A., Pichora, D.R., and Small, C.F. Developement of a Three Dimensional Finite Element Model for Carpal Load Transmission in a Static Neutral Posture, Annals of Biomedical Engineering, 2003, 31, 718–725.

13. Guo, X., Fan, Y., Li, Z.M., Effects of Dividing the Transverse Carpal Ligament on the Mechanical Behaviour of the Carpal Bones under Axial Compressive Load: A Finite Element Study, Medical Engineering & Physics, 2009, 31, 188-194.

14. Materialise, Mimics Help Manual, Materialise, version 12.1, 2008.

15. Ito, Y., Shum, P.C., Shih, A.M.,Soni, B.K. and Nakahashi, K.: Robust Generation of High-Quality Unstructured Meshes on Realistic Biomedical Geometry, International Journal for Numerical Methods in Engineering, 2006, 65, 943–973.

16. Louis, O., Willnecker, J., Soykens, S., Van den Winkel, P., Osteaux, M.: Cortical Thickness Assessed by Peripheral Quantitative Computed Tomography: Accuracy Evaluated on Radius Specimens, Osteoporosis International, 1995, 5, 446-449.

17. Simulia, Abaqus Theory Manual, Chapter. 2.4.5, Abaqus Inc, 2007, v.6.7-1.

18. Kauer, J.M., The mechanism of the carpal joint, Clinical Orthopaedics and Related Research, 1986, 202, 16–26.

19. Viegas, S.F., Patterson, R.M., P.D. Todd, P.D. and McCarty, P.: Load Mechanics of the Midcarpal Joint, Journal of Hand Surgery, 18A(1), 14-18, 1993.

20. Rho, J.Y., Ashman, R.B. and Turner, C.H.: Young's modulus of trabecular and cortical bone material: Ultrasonic and microtensile measurements, Journal of Biomechanics, 1993, 26(2), 111-119.

21. Rho, J.Y., Tsui, T.Y and Pharr, G.M.: Elastic properties of human cortical and trabecular lamellar bone measured by nanoindentation, Biomaterials, 1997, 18(20), 1325- 1330.

22. Brown , C.P., Nguyen, T.C., Moody, H.R., Crawford, R.W. and Oloyede A.: Assessment of Common Hyperelastic Constitutive Equations for Describing Normal and Osteoarthritic Articular Cartilage, Proc. IMechE Part H, Engineering in Medicine, 2009, vol 223, 6, 643-652.

23. Li, Z., Kim, J.E., Davidson, J.S., Etheridge, B.S., Alonso, J.E. and Eberhardt, A.W.: Biomechanical Response of the Pubic Symphysis in Lateral Pelvic Impacts: A Finite Element Study, Journal of Biomechanics 2007, 40, 2758-2766.

24. Finlay, J.B. and Repo, R.U.: Energy Absorbing Ability of Articular Cartilage During Impact, Medical and Biological Engineering and Computing, 1979, 17, 397-403.

25. Leanne, V.B. and Aspden, R.M.: Impact Testing to Determine the Mechanical Properties of Articular Cartilage in Isolation and on Bone, Journal of Material Science: Materials in Medicine, 2008, 19, 703-711.

26. Berger, R. A. The ligaments of the wrist: a current overview of anatomy with considerations of their potential functions. Hand Clin., 1999, 13, 63–82.

27. McGrouther , D.A. and Higgins, P.O., Interactive Hand - Anatomy CD, Primal Pictures, v.1.0

28. Bettinger, P. C., Linscheid, R. L., Berger, R. A.,Cooney, W. P., and An, K. N. An anatomic study of the stabilizing ligaments of the trapezium and trapeziometacarpal joint. J. Hand Surg. Am., 1999, 24(4), 786–798.

29. Bettinger, P. C., Smutz, W. P., Linscheid, R. L., Cooney, W. P., and An, K. N. Material properties of the trapezial and trapeziometacarpal ligaments. J.Hand Surg. Am., 2000, 25, 1085–1095.

30. Logan, S. E. and Nowak, M. D. Distinguishing biomechanical properties and intrinsic and extrinsic human wrist ligaments. Trans. ASME, J.mech. Eng, 1991, 113(1), 85–93.

31. Fowler, N.K. and Nicol, A.C., Interphalangeal Joint and Tendon Forces: Normal Model and Biomechanical Consequences of Surgical Reconstruction, Journal of Biomechanics, 2000, 33, 1055-1062.

32. Fowler, N.K. and Nicol A.C., Functional and Biomechanical Assessment of the Normal and Rheumatoid Hand, Clinical Biomechanics, 2001, 16(8), 660-666.

33. Shin, A.Y., Disruption of the Distal Carpal Row: Axial Carpal Instability and Dislocations of the Carpometacarpal Joint, Excluding the Thumb, 'Hand Surgery', editors Berger, R.A., Weiss, A-P, C., Volume 1, Lippincott, Williams and Wilkins, 2003, 533-549

34. Horii, E., An K.N. and Linscheid R.L.: Excursion of Prime Wrist Tendons, Journal of Hand Surgery, 1993, 18A, 83-90.

35. Johnson, R.P. and Carrera, G.F.: Cronic Capitolunate Instability, The Journal of Bone and Joint Surgery, 1986, 68: 1164-1176.

36. Harewood, F. J. and McHugh, P. E.: Comparison of the Implicit and Explicit Finite Element Methods Using Crystal Plasticity, Computational Materials Science, 2007, 39, 481-494.

37. Gislason, M., Nash, D.H., Nicol, A., Kanellopoulos, A., Bransby-Zachary, M., Hems, T.E.J., Condon, B., Stansfield, B.: A Three Dimensional Finite element Model of Maximal Grip Loading in the Human Wrist, Proc. IMechE Part H, Engineering in Medicine, Vol 223, (In press)